

Fatigue analysis of railway wheel using a multiaxial strain-based critical-plane index

M. Kiani  | G.T. Fry 

Zachry Department of Civil Engineering,
Texas A&M University, College Station,
TX 77840, USA

Correspondence

M. Kiani
Email: maysam@tamu.edu

Abstract

A fatigue damage model to assess the development of subsurface fatigue cracks in railway wheels is presented in this paper. A 3-dimensional finite element model (FEM) is constructed to simulate repeated cycles of contact loading between a railway wheel and a rail. The computational approach includes a hard-contact over-closure relationship and an elastoplastic material model with isotropic and kinematic hardening.

Results from the simulation are used in a multiaxial critical-plane fatigue damage analysis. The employed strain-based critical-plane fatigue damage approach is based on Fatemi-Socie fatigue index that takes into account the non-proportional and out-of-phase nature of the multiaxial state of stress occurs when a railway wheel rolls on a rail. It predicts fatigue-induced micro-crack nucleation at a depth of about 3.7 mm beneath the wheel tread, as well as the crack plane growth orientation which indicates the possible failure pattern. Additionally, the influence of various factors such as contribution of normal stresses, higher wheel load, and material model have been investigated.

KEYWORDS

critical-plane approach, multiaxial fatigue, railway wheels, rolling contact fatigue (RCF), subsurface fatigue crack, vertical split rim (VSR)

1 | INTRODUCTION

Technological advancements in the railway industry have made it possible to significantly extend the fatigue life of wheels. Simultaneously, current economical and logistical

constraints demand increasing train speeds and load capacities that result in larger contact forces on wheels. As a result, longer wear periods, higher speeds, and larger loads have made fatigue the main cause of railway wheel replacement and re-engineering.¹

There are roughly 25 to 50 million railway wheels in operation in the world. Considering an annual failure rate of one in 1000, it means 25 000 to 50 000 wheel failures every year. It's obvious that if "failure" here means a complete fracture of the wheel the way the train to be inoperative, railways would not be an efficient method of transportation.²

According to the Union Pacific Railroad wheel fracture database, 65% of railroad wheel failures are caused by shattered rims,³ a form of subsurface initiated

Nomenclature: C_k , =initial kinematic hardening modulus; E , =modulus of elasticity; FS , =Fatemi-Socie fatigue index; G , =shear modulus; Q_∞ , =maximum change in the size of the yield surface; S , =deviatoric stress tensor at the material point of interest; b , =yield surface development rate; $\Delta\gamma_{max}$, =maximum shear strain range in a cycle; α^{dev} , =deviatoric part of the back-stress tensor; γ_k , =kinematic hardening modulus decreasing rate; $\dot{\epsilon}^{pl}$, =rate of plastic flow; $\dot{\epsilon}^{pl}$, =equivalent plastic strain rate; η , =normal coefficient (an empirical material constant); ν , =Poisson's ratio; σ_{lo} , =yield stress at zero plastic strain; σ_n , =maximum normal stress in a cycle; σ_y , =yield stress; τ'_f , =Fatigue strength coefficient

rolling-contact fatigue (RCF). This suggests a need for the development of models that can effectively predict RCF cracks. Effective predictions require computational tools and mathematical models that can accurately simulate actual material behavior and structural interactions due to contact between railway wheels and rails.

Wheels constitute a fundamental component in railways; without them, the directed motion of the railway wagons and their contents is not possible. The strategic location and function of wheels make them a component that is also critical to safety. The failure of wheels, which is structural in nature, can seriously compromise the integrity of the transport medium. The inability of railway wheels to resist the loads they are subjected to while in service can eventually result in damage to rails, sleepers, the train's suspension, and/or bearings, and in some cases, can even result in derailments.

1.1 | Description of fatigue cracks in railway wheels

Surface cracks on wheel treads, ie, shelling and spalling, are due to localized plastic deformation of material close to wheel-rail interface. Kapoor⁴ suggests that either low-cycle fatigue (LCF) or ratcheting can be the failure mode of material in this region (their failure mechanisms are independent from each other).

In contrast to surface cracks, subsurface cracks nucleate at some depth below running surface where material deforms elastically; therefore, the mode of failure of subsurface cracks is the high-cycle fatigue (HCF).

1.2 | Subsurface fatigue

Crack initiation below the surface tends to take place at approximately 3 to 10 mm below the wheel rolling-surface,⁵ where the largest shear stresses due to rolling occur. When the fatigue process is initiated within this region, it is known as subsurface fatigue. In this subsurface region, although material plasticity and hardening may occur initially even at moderate load levels,⁶ at some point, the development of residual stresses may allow for the material to respond elastically in what is known as elastic shakedown. In regions of elastic shakedown, the fatigue phenomenon is of the high-cycle type.

1.3 | Engineering assessment of subsurface fatigue

Microscopy of fatigue cracks has shown that fatigue damage may initiate at depths of 3 to 4 mm below the tread surface, a zone where plasticity and wear represent

competing damaging mechanisms. Metallographic examinations like these suggest that shear cracking is responsible for RCF initiation once it exceeds fatigue-crack growth thresholds under the combined influence of normal and tangential forces.⁷

The present study comprises 2 analytical procedures to provide an adequate numerical assessment of the subsurface RCF environment in railway wheels:

- Developing 3-D FE models to capture stresses/strains during wheel-rail rolling contact.
- Using the results of the stress analyses to perform fatigue assessment of the wheel at subsurface level.

1.4 | Critical-plane models

Critical-plane approaches have been proposed for fatigue analysis of components with non-proportional multiaxial loading.⁸⁻¹⁰ Non-proportional loading results in the rotation of the principal stress axes as well as the maximum shear stress/strain amplitude planes at a given material point. Cracks are expected to eventually initiate on planes and at material points where a particular fatigue-damage parameter is maximized during the load cycle. It is a fundamental task in critical-plane approaches to search for the plane(s) that displays the highest fatigue damage at several or, ideally, all of the material points in a structural component during a loading cycle.

Critical-plane models evolved from experimental observations of the crack initiation and growth patterns in solids under cyclic loading. Experimental results show that, for commonly used metallic materials, fatigue crack first occurs along the crystal slip and then propagates perpendicular to the maximum principal stress direction. The fatigue fracture plane is the crack plane observed at the macro level, and critical plane is a material plane on which the fatigue damage is evaluated.¹¹

Critical-plane models should incorporate accurate constitutive parameters governing crack initiation and growth so that they can successfully predict the crack initiation location as well as the possible orientation of the failure planes.¹²⁻¹⁴

1.5 | Objective of the work

This work is focused on HCF damage under rolling contact. The purpose of this study is to propose a methodology that is able to provide a relatively accurate numerical prediction of the subsurface crack initiation location and its possible failure pattern based on the crack plane orientation in a “defect free” railway wheel. Full-scale numerical simulations of a wheel and rail setup

were performed, and stress/strain histories were recorded. The captured results have been then used as the input to the developed algorithm based on the critical-plane approach to analyze the wheel and to detect the fatigue hot spots. The paper is structured chronologically to reflect the overall progress of the work carried out within the project.

2 | NUMERICAL SIMULATION TO RECORD STRESS/STRAIN HISTORIES

Most fatigue models rely on stress and strain input values to produce their predictions. In this study, time-history contact-stress analyses of a railway wheel rolling on a rail segment are performed using a 3D FE model. The results of these analyses are later used in a multiaxial strain-based fatigue model to estimate the location as well as the orientation of the first subsurface fatigue-induced micro-crack. It's been noted in previous studies that strain-life approach used along with elastic-plastic FE analysis makes a powerful combination in prediction of fatigue crack initiation.¹⁵ The details of the constructed FE model are described in the following sections. The effect from temperature resulting from friction has been disregarded in the simulations, as it was beyond the scope of the current study. Additionally, the effect/behavior of the subsurface residual stresses and strains will be thoroughly presented in another paper.

2.1 | Material model

In wheel/rail contact, plastic deformation usually occurs even at fairly moderate load levels.⁶ Plastically deformed material experiences plastic hardening as well as accumulation of residual stresses. Due to these 2 effects, a load magnitude that causes plastic deformation may, after some load cycles, only cause elastic response. This effect is called *elastic shakedown*. With a more severe

loading, the cyclic stress/strain curve becomes a stabilized closed loop with zero total plastic deformation. Such a material response is called *plastic shakedown*. Finally, when every load cycle causes additional plastic deformation and the deformation exceeds the material ductility, the material response is called *ratchetting* or cyclic creep (Figure 1).

Due to heavy axle loads in locomotive industry, localized plastic deformation occurs at the wheel-rail contact interface.¹⁶ Such a compressive deformation at running surface is balanced by tensile residual stresses at subsurface, which are found to play an important role in fatigue crack nucleation.¹⁷ The stress-strain relationship for all the components in the FE model is defined using a plasticity model with both isotropic and kinematic hardening.¹⁸

Johansson and Thorbemtsson¹⁹ developed an optimization algorithm—based on some test results by Bower²⁰ on rail steels—to calibrate parameters for the Chaboche plasticity model. The optimization result showed an accurate ratchetting prediction with some deviation of the shape in stress-strain plots. Using stress-strain plots of specific loading cycles, Ringsberg et al²¹ later used this optimization results to determine Chaboche model parameters and implemented it into ABAQUS material library to study FEA of rolling contact. Due to less complexity of the Chaboche plasticity model, it is more suitable for studying FEA of computationally intensive full-scale wheel rail contact.¹⁷

In general, isotropic and kinematic hardening rules are coupled in plasticity models. The isotropic hardening rule predicts change of the size of yield surface as plastic deformation evolves, while the kinematic hardening rule is responsible for the translation of yield surfaces—called the *Bauschinger effect*—due to cyclic load. The kinematic hardening rule also controls the ratchetting behavior of material.

The yield criterion in the model uses the von Mises equivalent stress concept, according to which a material point is considered to reach its yield point when the second invariant of the deviatoric stress tensor at that

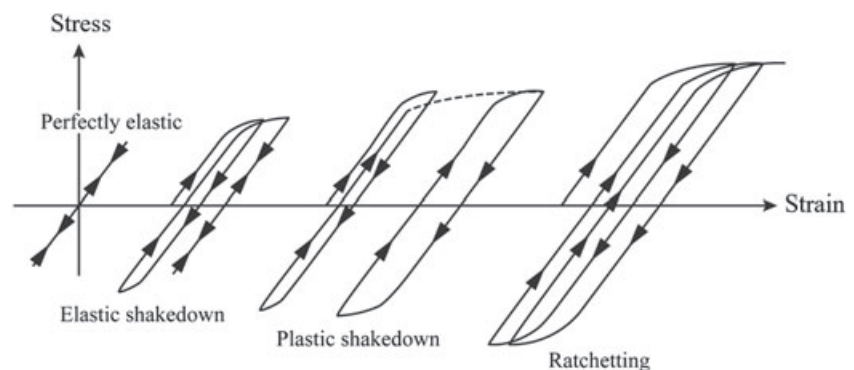


FIGURE 1 Illustration of different material responses: (A) perfectly elastic; (B) elastic shakedown; (C) plastic shakedown; (D) ratchetting

point equals the square of the yield stress of the material. Thus, the yield surface is defined by:

$$F = \sqrt{\frac{3}{2}(\mathbf{S} - \boldsymbol{\alpha}^{dev}) : (\mathbf{S} - \boldsymbol{\alpha}^{dev})} - \sigma^0 = 0 \quad (1)$$

where \mathbf{S} corresponds to the deviatoric stress tensor at the material point of interest, and $\boldsymbol{\alpha}^{dev}$ is the deviatoric part of the back-stress tensor.

Kinematic hardening models assume associated plastic flow, which is given by:

$$\dot{\boldsymbol{\epsilon}}^{pl} = \dot{\bar{\boldsymbol{\epsilon}}}^{pl} \frac{\partial F}{\partial \boldsymbol{\sigma}} \quad (2)$$

where $\dot{\boldsymbol{\epsilon}}^{pl}$ is the rate of plastic flow and $\dot{\bar{\boldsymbol{\epsilon}}}^{pl}$ is the equivalent plastic strain rate. This latter is obtained from the performed plastic work,

$$\sigma^0 \dot{\bar{\boldsymbol{\epsilon}}}^{pl} = \boldsymbol{\sigma} : \dot{\boldsymbol{\epsilon}}^{pl} \quad (3)$$

which yields $\dot{\bar{\boldsymbol{\epsilon}}}^{pl} = \sqrt{\frac{2}{3} \dot{\boldsymbol{\epsilon}}^{pl} : \dot{\boldsymbol{\epsilon}}^{pl}}$ for isotropic Mises plasticity. The kinematic hardening law is then given as follows:

$$\dot{\boldsymbol{\alpha}}_k = C_k \frac{1}{\sigma^0} (\boldsymbol{\sigma} - \boldsymbol{\alpha}) \dot{\bar{\boldsymbol{\epsilon}}}^{pl} - \gamma_k \boldsymbol{\alpha}_k \dot{\bar{\boldsymbol{\epsilon}}}^{pl} \quad (4)$$

where C_k is the initial kinematic hardening modulus, and γ_k determines the rate at which the kinematic hardening modulus decreases with increasing plastic deformation.

The isotropic hardening law is given by:

$$\sigma^0 = \sigma|_0 + Q_\infty \left(1 - e^{-b \bar{\boldsymbol{\epsilon}}^{pl}}\right) \quad (5)$$

where $\sigma|_0$ is the yield stress at zero plastic strain, Q_∞ is the maximum change in the size of the yield surface, and b defines the rate at which the size of the yield surface changes as plastic straining develops.

Characterizations of the cyclic behavior of railway-wheel-specific materials are very limited and/or have not been sufficiently detailed for their analytical application in the Chaboche plasticity model with combined isotropic and kinematic hardening. On the other hand, the experimental determination of the wheel's material properties in terms of the utilized plasticity model is beyond the objectives of this study. Accordingly, the material properties and hardening parameters for pearlitic rail steel used in this study are given below¹⁷:

Modulus of elasticity, $E = 209$ GPa

Poisson's ratio, $\nu = 0.29$

Initial yield stress, $\sigma|_0 = 406$ MPa

Initial kinematic hardening modulus, $C_k = 13.2$ GPa

Kinematic hardening modulus decreasing rate,

$\gamma_k = 3.12$

Maximum change in the size of the yield surface, $Q_\infty = 152$ MPa, and

Yield surface development rate, $b = 3.97$

To capture the most possible realistic response of the wheel, material nonlinearity as well as geometrical nonlinearity are taken into account by using Chaboche plasticity model and *Nlgeom* keyword in ABAQUS, respectively.

2.2 | Finite element modeling of wheel/rail contact

The programs used for modeling (preprocessing) and performing the required FE analyses are HyperMesh^{®22} and ABAQUS^{®,23} respectively. The FE model (Figure 2) comprises a single railroad wheel, a contributory portion of the axle that it is attached to, and a rail segment with profiles provided by the American Association of Railroads (AAR). The wheel has a diameter of 914 mm and is modeled under 2 vertical loads of 162 and 233 kN to capture the effect of different loading on subsurface fatigue crack behavior. The loads correspond to a realistic weight estimation that is amplified to account for dynamic effects. The force is applied at a point on the longitudinal axis of the axle that is located where the wagon is supported. The contributory length of the axle in the FE model corresponds to half its actual length, which accounts for the symmetry of the actual wheel-axle

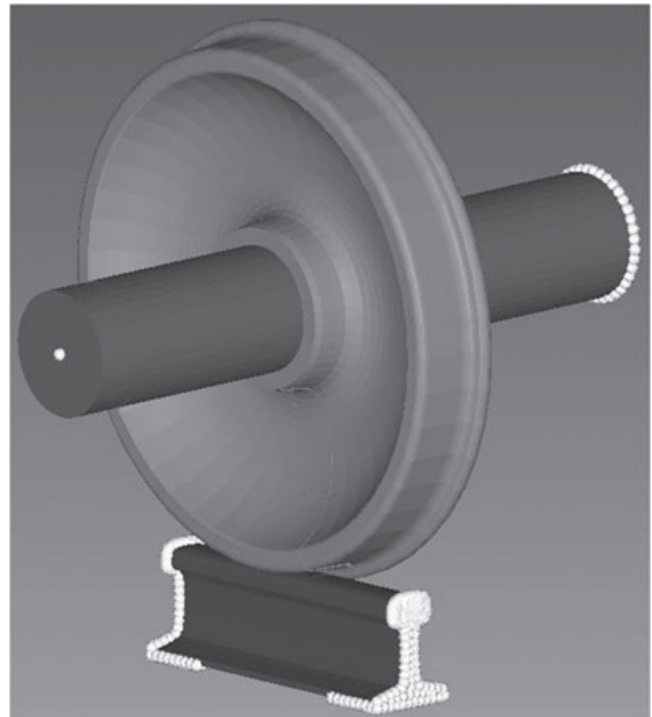


FIGURE 2 FE model and its boundary conditions²⁴

assembly. The rail segment has a length of 600 mm, which is a typical practical distance between ties/sleepers.

In the finite element model (FEM) snapshot given in Figure 2, the portion of the mesh denoted in white is subjected to the following boundary conditions. Due to symmetry, the displacements along the longitudinal axis of the axle are restrained at the end of the contributory axle corresponding to the middle of the actual axle; the rail is restrained at its ends on its longitudinal axis to also account for symmetry and continuity with the rest of the “infinite” rail. Portions of the bottom of the rail are fixed at the locations where the rail segment is assumed to make contact with the ties. Although, in reality, this latter is a contact boundary condition, fixing the nodes is justified because the effects of the fixities of these nodes on the stress response of the wheel are minimal.

The type of element used in the mesh is an 8-noded reduced-integration solid (ABAQUS C3D8R element-type); that is, linear interpolation is used between nodal values for the primary variables as well as for the geometry. The selection of an element with linear interpolation was made because second-order elements can cause problems when hard contact between elements is enforced (as it is in this study) because of the way consistent nodal pressure loads are calculated.

For accuracy, precision, resolution, and numerical efficiency, the FE mesh in the wheel's and rail's regions in the vicinity of the contact areas were greatly refined. Figures 3 and 4 illustrate the level of mesh refinements performed in the regions adjacent to the areas that are expected to make contact as well as the 70-mm rolling trajectory. The element size in the refinement area is approximately 1.3 mm wide \times 1.4 mm deep \times 2 mm long in the wheel and rail. In total, the FE mesh is made up by about 340 000 elements.

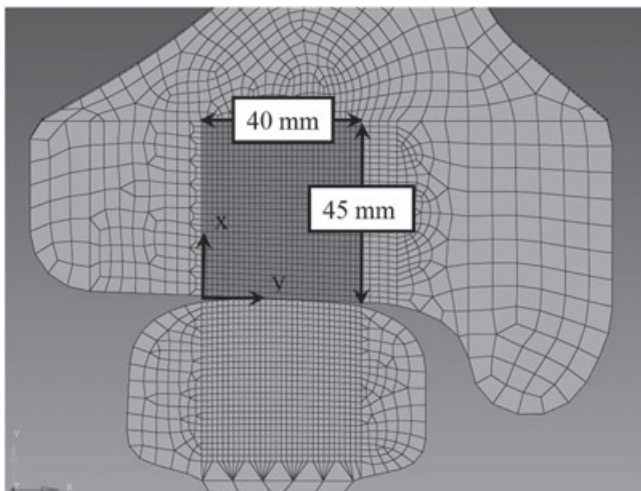


FIGURE 3 Wheel/rail mesh in the region of contact

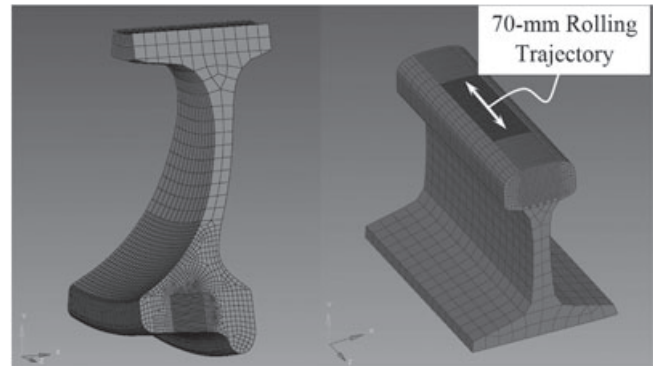


FIGURE 4 Mesh refinement in the region of contact and the rolling trajectory

The element size around the areas of contact was, in part, selected in consideration of this master-slave relationship. The friction coefficient specified for surface interaction is 0.3, which has been commonly employed in steel-to-steel rolling-contact analytical studies.²⁵

2.3 | Loading steps to simulate rolling contact

The rolling of the wheel is performed in a distance of 70 mm with 1-mm increments. A previously carried-out FE study on the RCF of rails that uses the same wheel and rail profiles¹⁷ determined that this rolling distance was sufficient to capture the “full” stress/strain response that takes place during rolling at any component cross section. Therefore, in this study, the evaluation of the stress/strain response and of the modeled wheel is performed at a cross section located in the middle of the rolling trajectory of the wheel; that is, the wheel cross section that is most directly in contact with the rail once the wheel has been rolled a distance of 35 mm.

The inelastic nature of materials, and particularly that of steel, produces residual stresses and strains as a byproduct of their cyclic response. As wheels roll on a rail, the yield surfaces of the material indicate that they expand and translate until they reach a final (steady-state) configuration. This is not only a result of the material model that is used, but the representation of what happens in reality when plastic materials respond in their inelastic range.

The predicted steady-state stress/strain response is reached quickly; therefore, railway wheels and rails respond steadily during virtually their whole service life. This is why any study involving rolling contact between wheels and rails needs to be performed based on stabilized material conditions (ie, constant residual stress state). If stresses and strains corresponding to the very first cycle (s) were used, different fatigue-life predictions would be obtained depending on the cycle chosen for the application

of the fatigue model. These would most likely be in disagreement with field and experimental tests.

To reach the steady state of stress/strain response in the constructed FE model, the wheel is rolled several times on the rail until analytical evidence exists that the stress-strain response of the material has been stabilized (within an acceptable range). A plot of the residual-stress progression at a node located approximately 15 mm below the running surface (see Figure 5) of the wheel is given in Figure 6. The residual stresses in the wheel are essentially stabilized after the fifth cycle, which agrees with the findings of Kabo and Ekberg.²⁶ Because of the periodic nature of the contact loads between the wheel and rail, this at-the-end-of-cycle stabilization indicates a reached state of either elastic or plastic shakedown. In any case, stress/strain time-histories obtained from any cycle after

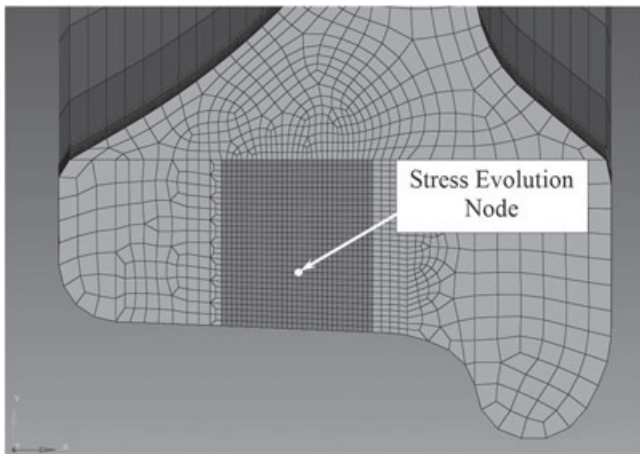


FIGURE 5 Locations of stress evaluation node

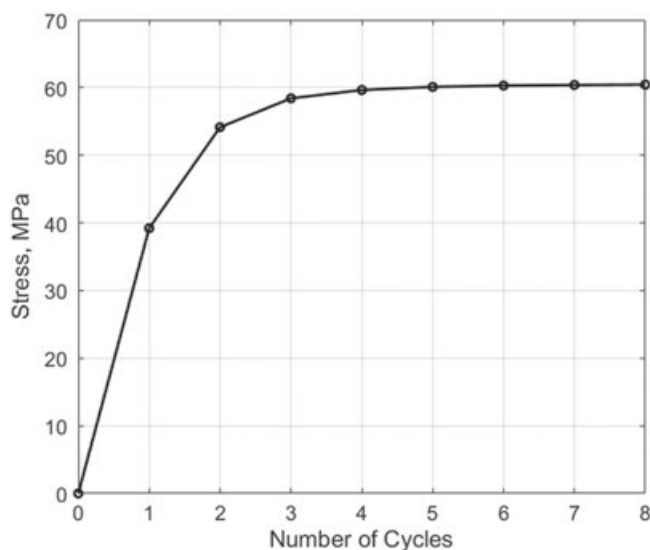


FIGURE 6 Predicted cyclic residual stress evolution in the wheel

the fifth one can be used for the fatigue analysis of the wheel. In this study, the data from the sixth loading cycle are used in the prediction of the fatigue-related results. Although, the elastic limit of the material is exceeded in a significant region of the wheel, the stress field did not reach values that were much greater than the material's yield stress (Figure 7). Additionally, state of elastic shakedown is predicted by the model in some regions which is in agreement with the theoretical study of Bower and Johnson.¹⁶

3 | FATIGUE DAMAGE ANALYSIS USING A STRAIN-LIFE CRITICAL-PLANE FATIGUE CRITERION

Fatigue cracks nucleate primarily on planes of maximum shear and usually grow on the plane of maximum tensile stress. At the microscopic level, cracks usually have irregular shape while they grow which results in interlocking and friction forces between crack faces as illustrated in Figure 8A. Consequently, the crack tip driving force is reduced, and the fatigue life is increased. A tensile stress perpendicular to the crack plane tends to separate crack faces which reduce interlocking and frictional forces, as shown in Figure 8B. This increases the crack tip driving force, and the fatigue life is reduced.^{27,28}

3.1 | Crack initiation prediction

The philosophy of the total-life methods is to estimate the resistance to fatigue crack nucleation based on

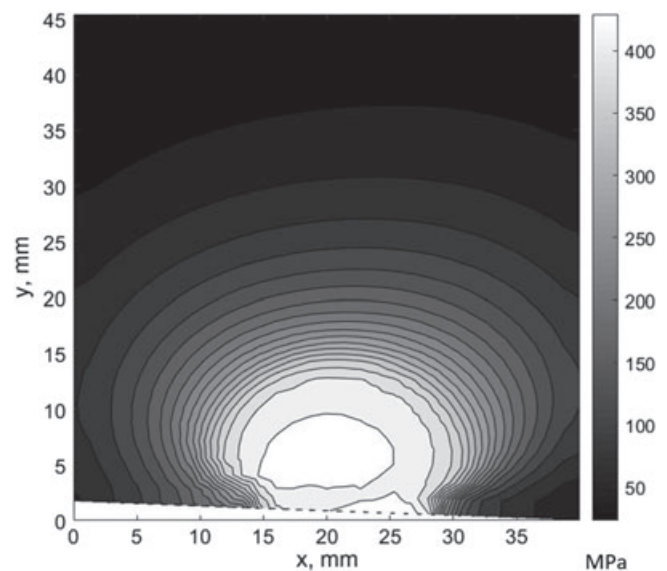


FIGURE 7 Predicted peak von Mises contact-stress response at the wheel's cross section during the sixth load cycle

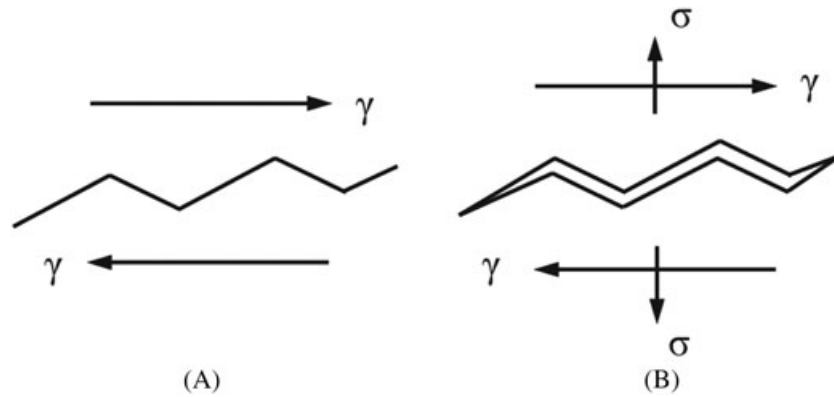


FIGURE 8 Physical basis of the Fatemi-Socie model

nominally defect-free parts. A drawback to the total-life method is that the definition of failure is not clear.¹⁵ These methods analyze the total fatigue life to failure (crack nucleation in this case) and are divided into stress-based and strain-based approaches. The stress-based (stress-life) approach is characterized in terms of low cycle stress ranges that are designed against fatigue crack initiation (HCF failures). However, at high load levels, in the low cycle fatigue (LCF) regime, the cyclic stress-strain response and the material behavior are best modeled under strain-controlled conditions (strain-life approach).²⁹ The stresses in this approach are high enough to cause plastic deformations that governs fatigue failure (LCF failure).

A strain-based approach is employed in the current study. The strain-life approach used along with FE analyses makes a powerful combination because any arbitrary geometry with any material and loading can be analyzed for fatigue as long as the stress/strain fields can be captured from FE analyses (there is no need for assuming crack size, location, and orientation).

3.2 | Fatemi-Socie fatigue criterion

This section is concerned with the implementation of a strain-based critical-plane criterion to estimate the fatigue-initiation life of the railway wheel of the FE model. For this purpose, the sixth loading cycle of the stress/strain response time-history obtained from the FE model is imported into MatLab[®] wherein the Fatemi-Socie fatigue criterion was coded as a computer algorithm. This is a multiaxial strain-based critical-plane criterion that can account for plastic behavior and can therefore be applied to the HCF and LCF regimes.¹⁷

The model employed herein, originally proposed by Fatemi and Socie,³⁰ is represented by the following equation:

$$FS = \frac{\Delta\gamma_{\max}}{2} \left(1 + \eta \frac{\sigma_{n,\max}}{\sigma_y} \right) \quad (6)$$

where $\Delta\gamma_{\max}$ is the maximum shear strain range in a cycle, $\sigma_{n,\max}$ is the maximum normal stress in a cycle, η is the normal coefficient, which is an empirical material constant, and FS is the Fatemi-Socie fatigue index.

The basis of the Fatemi-Socie (FS) model²⁷ is that the irregular shapes of crack surfaces produce friction forces that oppose shear deformations along the crack's plane. This mechanism impedes crack growth, thereby increasing the fatigue life of the material. If tensile stresses normal to the plane of the crack are present, they reduce the normal forces on the crack surfaces, thereby also reducing the friction forces acting on the crack faces. If this reduction in the friction forces takes place, the crack tips must carry a greater fraction of the far-field shear forces, which is assumed to favor the growth of the crack.

The FS model accounts for the interaction between cyclic shear strain and normal stress at a particular material point on a particular plane during a cycle of load. The normal stress across a plane accounts for the influence of friction.

The material-dependent coefficient term used to include the influence of normal stress on the FS fatigue criterion is called the normal coefficient (η) in this study. The value of normal coefficient for pearlitic rail steel is determined from a regression analysis between the FS fatigue index and fatigue life data from the literature.¹⁷

In order to find the plane with the maximum FS fatigue index, an exhaustive search using the spherical coordinate throughout all possible planes is performed by varying the elevation (φ) and azimuth (θ) angles (Figure 9). However, to avoid excessive run time in both data processing and optimization steps, the plane search is performed with 10° increments of both φ and θ . The normal vector that defines a plane can be written as follows:

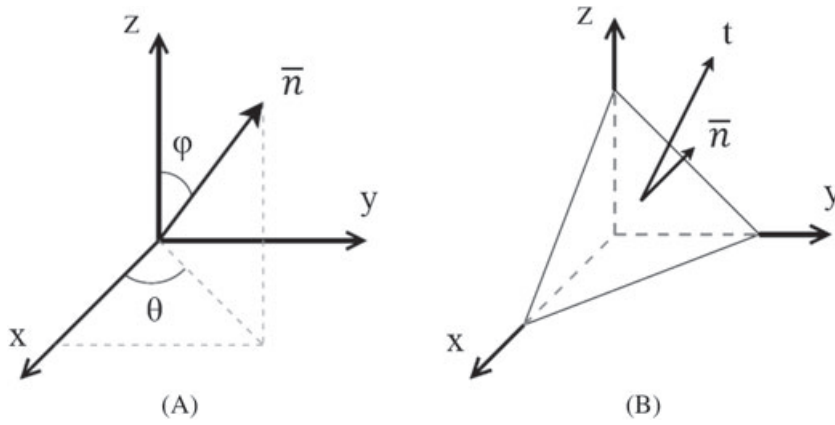


FIGURE 9 (A) The spherical coordinate; (B) traction vector on each critical plane (Cauchy's law)

$$\bar{n} = \begin{Bmatrix} n_1 \\ n_2 \\ n_3 \end{Bmatrix} = \begin{Bmatrix} \sin\varphi \cos\theta \\ \sin\varphi \sin\theta \\ \cos\varphi \end{Bmatrix} \quad (7)$$

4 | RESULTS AND DISCUSSION

4.1 | Fatigue index of the 162-kN wheel load with material hardening

For each node in the $40 \times 45 \text{ mm}^2$ region of Figure 3 (based on the defined x and y coordinates), the *FS* fatigue

index is calculated using the developed algorithm in MatLab® from a stress and strain tensor history for all selected planes. Among those planes, contours of the largest fatigue indices for different normal coefficient (η) values are illustrated in Figure 10.

Figure 10A illustrates the maximum *FS* fatigue damage index for $\eta = 0$, that is, the crack nucleates solely by shear strain amplitude effect. The fatigue index is concentrated in an area of 4 to 7 mm beneath the wheel tread with the maximum fatigue index of 0.0013755 at 3.7 mm depth. When $\eta = 1$ (participation of normal stress), the fatigue index is still around the same area,

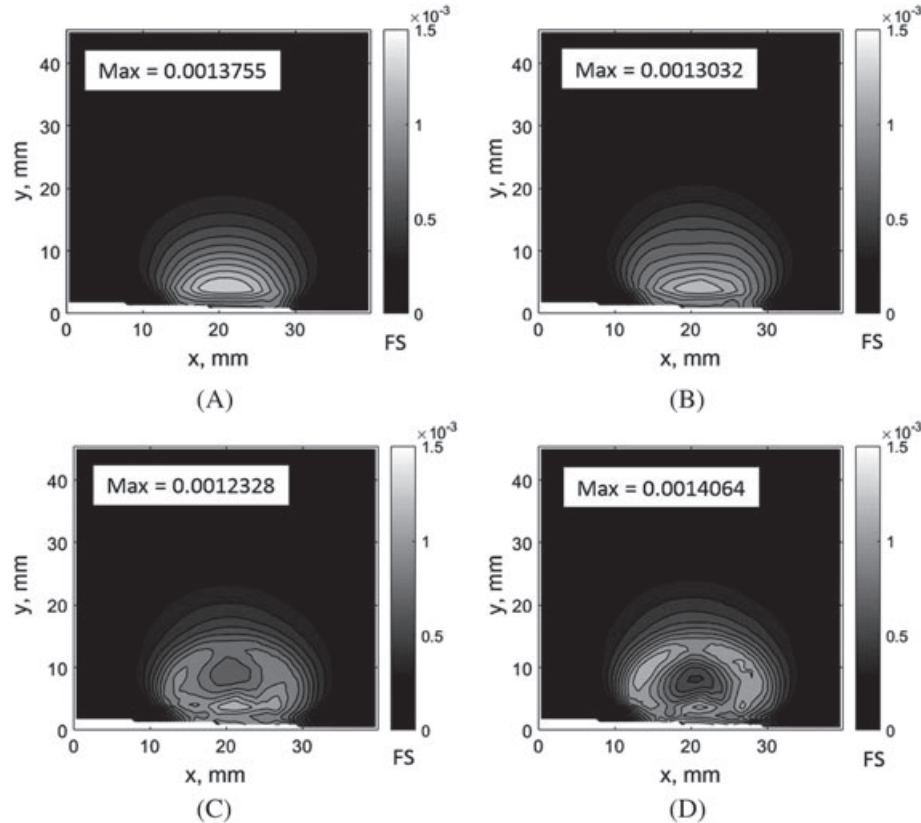


FIGURE 10 Maximum *FS* fatigue index contour of the 162-kN wheel load with hardening material: (A) $\eta = 0$, (B) $\eta = 1$, (C) $\eta = 3$, and (D) $\eta = 5$

TABLE 1 Summary of possible fatigue crack nucleation sites and cracking planes for the 162-kN wheel load with material hardening and different η values

Normal coefficient (η)	FS fatigue index	Depth below running surface (mm)	Unit normal vector of critical plane			Cracking plane
			x	y	z	
0	0.0013755	3.8	-0.72	-0.60	-0.34	Vertical/horizontal
1	0.0013032	3.7	0.49	-0.85	0.17	Horizontal/vertical
3	0.0012328	3.7	0.49	-0.85	0.17	Horizontal/vertical
5	0.0014064	0.5	0.00	0.00	1.00	Transverse

however with slightly lower peak value of 0.0013032 (Figure 10B). The fatigue index contour for $\eta = 3$ shows less localized damage site as opposed to 2 previous cases with the lower pick value of 0.0012328 (Figure 10C). Finally, for $\eta = 5$, Figure 10D shows multiple crack nucleation sites: at the surface and at a deeper depth of approximately 10 mm below running surface.

The value of η for perlitic wheel/rail steel has been evaluated by Tangtragulwong¹⁷ in a similar study on railheads. He determined η from a regression analysis between the FS fatigue index and fatigue life data of various loading configurations: uniaxial, torsion-axial, and bending, for rail steel. He concluded that the proper value of η is the one that produces the best linear fitting of a log-log plot between the FS fatigue index and fatigue life. Tangtragulwong calculation of η is in agreement with the results reported by Park and Nelson³¹ showing that η is varying from 0 to 2 for different types of steel. Jiang et al³² considered 0.98 for S460 N steel, and also Stephens et al²⁸ recommended $\eta = 1$ for a first approximation when fatigue test data are not available. Although the value of η expects to be from 0 to 2, in this study, the higher limit is extended to 5 to observe its general trend as well as micro-crack nucleation behavior during higher contribution of normal stresses.

Table 1 summarizes the predicted crack depth and the approximated corresponding cracking plane for different normal coefficients. For pearlitic rail/wheel steel ($\eta = 1$), the value of $y = 3.7$ mm corresponds to a fatigue-crack initiation depth of approximately 3 mm, which is consistent with the findings of previous research.⁵ In particular, Ekberg et al³³ illustrated a sketch of morphology of a real fatigue crack initiated in approximately 4 mm below the surface which qualitatively follows the same crack growth pattern as the FS index in current study predicted. Quantitative comparison and correlating this criterion to the number of cycles to failure require extensive field tests and consideration of other factors that are beyond the scope of this study.

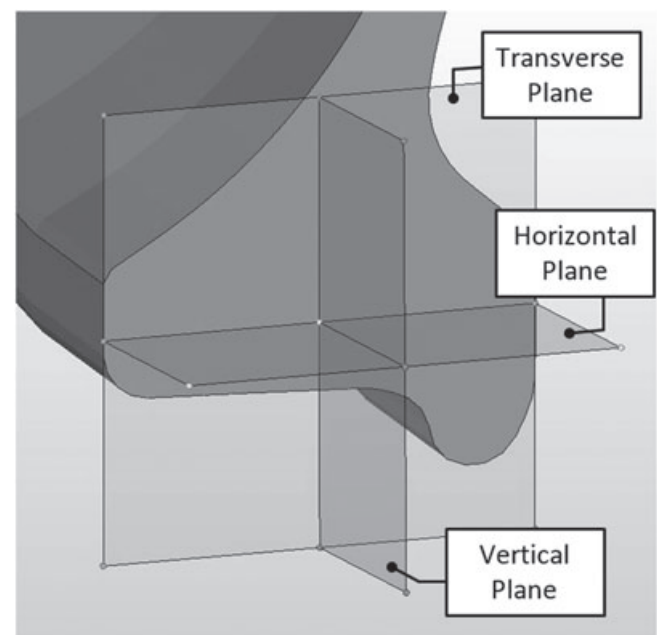
The cracking plane is defined based on Figure 11: for pearlitic rail/wheel steel ($\eta = 1$), it's a mixed horizontal/vertical plane (more inclined to horizontal than vertical). Prediction of 2 near-surface fatigue crack nucleation sites

in the case of $\eta = 3$ and 5 as opposed to only 1 site in the cases of $\eta = 0$ and 1 shows the importance of the effect of the normal stress components.

4.2 | Effect of higher wheel load on FS fatigue index

Figure 12 illustrates the FS fatigue index contours during the sixth cycle of a rolling contact of the 233-kN wheel load as η equals 0, 1, 3, and 5. In all cases, fatigue index increased compared with corresponding 162-kN cases with the same depth of crack nucleation site. Multiple fatigue nucleation sites are observed in cases of η equal to 3 and 5. In these cases, the crack nucleation sites in approximate depth of 10 to 15 mm under the running surface of the wheel are predicted.

The crack nucleation depths, direction cosines of critical planes, and corresponding FS fatigue indices of possible crack nucleation sites for all different normal coefficients (η) are summarized in Table 2. Results are

**FIGURE 11** Planes of propagation for wheel subsurface crack

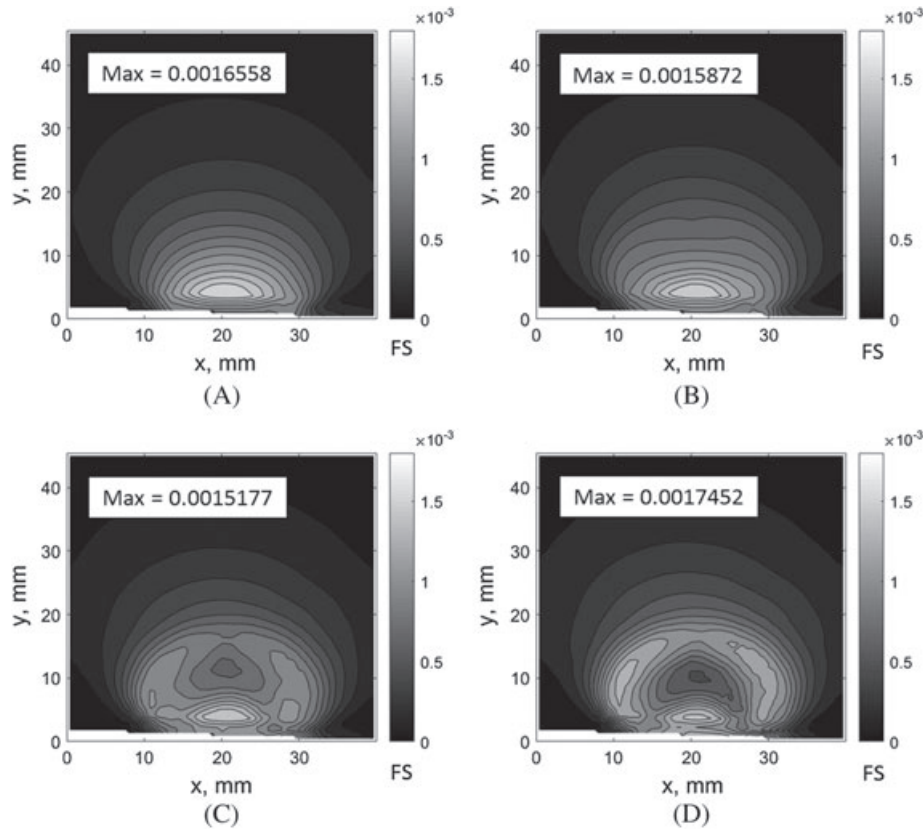


FIGURE 12 Maximum FS fatigue index contour of the 233-kN wheel load with hardening material: (A) $\eta = 0$, (B) $\eta = 1$, (C) $\eta = 3$, and (D) $\eta = 5$

qualitatively similar to those for 162-kN wheel load case, except for $\eta = 1$ case where a vertical plane is predicted as critical plane of crack propagation. The more vertical crack propagation plane means the initiated crack reaches the wheel surface in a steeper plane. In other words, it reaches the wheel tread faster, hence more imminent wheel failure.

4.3 | Effect of material hardening on FS fatigue index

Implementing elastic material as an input in the FE model instead of hardening material results in higher and more localized fatigue indices in all cases

(Figure 13). Fatigue index contours remain mainly unchanged as η increases from 0 to 5 with the maximum index of 0.0018257 for $\eta = 5$ case. Comparing Figures 10A and 13A (both cases of 162-kN wheel load with $\eta = 0$), the fatigue index increases from 0.0013755 in hardening case (consideration of strain accumulation) to 0.0017146 by using elastic material. A similar behavior is observed in the simulation with $\eta = 1, 3$, and 5 indicating the beneficial role of the strain accumulation on surface fatigue crack nucleation which contradicts the detrimental role of strain accumulation in failures due to ratcheting. In other words, accumulation of plastic deformation that results in ratcheting seems to be beneficial in controlling the high stress concentration

TABLE 2 Summary of possible fatigue crack nucleation sites and cracking planes for the 233-kN wheel load with material hardening and different η values

Normal coefficient (η)	FS fatigue index	Depth below running surface (mm)	Unit normal vector of critical plane			Cracking plane
			x	y	z	
0	0.0016558	3.8	-0.88	-0.32	-0.34	Vertical/horizontal
1	0.0015872	3.8	-0.97	-0.17	0.17	Vertical
3	0.0015177	3.8	0.49	-0.85	0.17	Horizontal/vertical
5	0.0017452	0.5	0.00	0.00	-1.00	Transverse

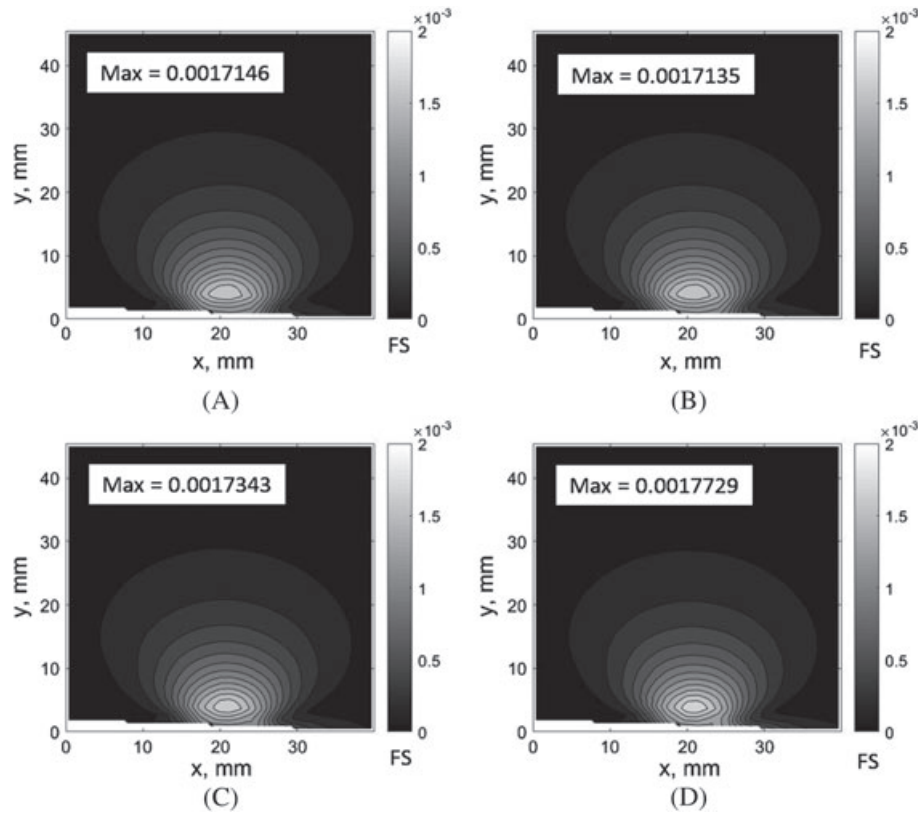


FIGURE 13 Maximum FS fatigue index contour of the 162-kN wheel load with elastic material: (A) $\eta = 0$, (B) $\eta = 1$, (C) $\eta = 3$, and (D) $\eta = 5$

occurs in the case with elastic material. This contradiction has also been observed in a similar study on rails by Tangtragulwong.¹⁷

5 | CONCLUSIONS

This paper has presented the results of analytical procedures focused on providing an adequate numerical assessment of fatigue-induced subsurface crack initiation behavior in railway wheels. Based on the numerically simulated local stress/strain histories within contact regions, a multi-axial strain-based critical-plane fatigue damage criterion is employed, and different influencing factors are discussed. The following conclusion can be drawn from our results:

1. Although the elastic limit of the material is exceeded in a significant region of the wheel, the stress field did not reach values that were much greater than the material's yield stress, and a state of elastic shakedown is predicted by the model in some regions.
2. The value of $y = 3.7$ mm corresponds to a fatigue-crack initiation depth of 3 to 10 mm, which is consistent with the findings of previous research.
3. The predicted crack propagation critical planes are almost similar in both wheel load cases with slight

difference in $\eta = 1$ case (pearlitic wheel/rail steel). In this case, the critical plane for higher wheel load is predicted to be more inclined to vertical plane. This could be due to higher tensile residual stresses at subsurface level which may increase the possibility of vertical split rim (VSR) failure in railway wheel subjected to higher wheel loads.

4. The presented approach shows various crack nucleation pattern for different normal coefficients. For $\eta = 0, 1$, and 3, the nucleation site is more localized, whereas in the $\eta = 5$ case (higher contribution of normal stresses), multiple nucleation sites are predicted (surface and subsurface).
5. The predicted crack plane orientation varies for different normal coefficients. Without the consideration of normal stress ($\eta = 0$), cracking plane is mostly vertical. This fatigue model predicts the crack growth more close to the horizontal plane for the pearlitic wheel/rail steel ($\eta = 1$).
6. The observed fatigue index reduction in using hardening material as opposed to elastic material indicates the beneficial role of the strain hardening on subsurface fatigue crack nucleation.

More work should be done to clarify the behavior of residual stresses and strains at the wheel's subsurface level.

ACKNOWLEDGEMENTS

The authors would like to acknowledge the support from University Transportation Center for Railway Safety (UTCRS) which funded this study through USDOT. Additionally, the help from Texas A&M University High Performance Research Computing (HPRC) facility that provided adequate resources to perform the highly exhaustive simulations in this work is greatly appreciated.

ORCID

M. Kiani  <http://orcid.org/0000-0001-9123-7895>

G.T. Fry  <http://orcid.org/0000-0002-8656-2308>

REFERENCES

- Ekberg A, Marais J. Effects of imperfections on fatigue initiation in railway wheels. *Journal of Rail and Rapid Transit*. 2000;214:45-54.
- Lewis R, Olofsson U. *Wheel–Rail Interface Handbook*. Woodhead Publishing Limited; 2009.
- Liu Y, Stratman B, Mahadevan S. Fatigue crack initiation life prediction of railroad wheels. *Int J Fatigue*. 2006;28:747-756.
- Kapoor A. A re-evaluation of the life to rupture of ductile metals by cyclic plastic strain. *Fatigue Fract Eng Mater Struct*. 1994;17:201-219.
- Ekberg A, Kabo E, Andersson H. An engineering model for prediction of rolling contact fatigue of railway wheels. *Fatigue & Fracture of Engineering Materials & Structures (FFEMS)*. 2002;25:899-909.
- A. Ekberg, "Rolling contact fatigue of railway wheels," Ph.D. Thesis, Department of Solid Mechanics, Ph.D. Thesis, Department of Solid Mechanics, Chalmers University of Technology, Goteborg, 2000.
- Mutton PJ, Epp CJ. Rolling contact fatigue in railway wheels under high axle loads. *Wear*. 1991;144:139-152.
- Meggiolaro MA, Castro JTP. Evaluation of multiaxial stress-strain models and fatigue life prediction methods under proportional loading. In: Da Costa Mattos HS, Alves M, eds. *Mechanics of Solids in Brazil 2009*. Rio de Janeiro, Brazil: Brazilian Society of Mechanical Sciences and Engineering; 2009.
- Carpinteri A, Spagnoli A, Vantadori S, Bagni C. Structural integrity assessment of metallic components under multiaxial fatigue: the C–S criterion and its evolution. *Fatigue & Fracture of Engineering Materials & Structures (FFEMS)*. 2013;36(9):870-883.
- Carpinteri A, Ronchei C, Spagnoli A, Vantadori S. On the use of the prismatic hull method in a critical plane-based multiaxial fatigue criterion. *Int J Fatigue*. 2014;68:159-167.
- Liu Y, Mahadevan S. Multiaxial high-cycle fatigue criterion and life prediction for material. *Int J Fatigue*. 2005;7(7):790-800.
- Carpinteri A, Fortese G, Ronchei C, Scorza D, Vantadori S. Spectral fatigue life estimation for non-proportional multiaxial random loading. *Theoretical and Applied Fracture Mechanics*. 2016;83:67-72.
- Carpinteri A, Fortese G, Ronchei C, Scorza D, Spagnoli A, Vantadori S. Fatigue life evaluation of metallic structures under multiaxial random loading. *Int J Fatigue*. 2016;90:191-199.
- Carpinteri A, Berto F, Campagnolo A, et al. Fatigue assessment of notched specimens by means of a critical plane-based criterion and energy concepts. *Theoretical and Applied Fracture Mechanics*. 2016;84:57-63.
- Ringsberg JW. Life prediction of rolling contact fatigue crack initiation. *Int J Fatigue*. 2001;23(7):575-586.
- A. F. Bower and K. L. Johnson, "Shakedown, residual stress and plastic flow in repeated wheel-rail contact," in *Rail Quality and Maintenance for Modern Railway Operation*, K. J. J., Ed.: Kluwer Academic Publishers, 1993, pp. 239--249.
- P. Tangtragulwong, "Optimal railroad rail grinding for fatigue mitigation," Ph.D. Dissertation, Department of Civil Engineering, Texas A&M University, College Station, TX, 2010.
- Chaboche JL. On some modifications of kinematic hardening to improve the description of ratchetting effects. *International Journal of Plasticity*. 1991;7, no. 7 SRC - GoogleScholar:661-678.
- A. Johansson and H. Thorbemtsson, "Elastoplastic Material Model with Nonlinear Kinematic Hardening for Rolling and Sliding Contact Fatigue," Technical Report EX, 1997.
- Bower AF. Cyclic hardening properties of hard-drawn copper and rail steel. *J Mech Phys Solids*. 1989;37, no. 4 SRC - GoogleScholar:455-470.
- Ringsberg JW, Bjarnehed H, Johansson A, Josefson BL. Rolling contact fatigue of rails—finite element modelling of residual stresses, strains and crack initiation. *Journal of Rail and Rapid Transit*. 2000;214:7-19.
- Altair, HyperMesh tutorials: abaqus solver interface. Altair Engineering Inc., 2014.
- Simulia. *ABAQUS 6.13 Analysis User's Manual*. Providence, RI: Dassault Systemes Simulia Corp; 2013.
- M. Kiani, "Multi-scale fatigue damage life assessment of a railway wheel using a critical-plane model," Ph.D. Dissertation, Department of Civil Engineering, Texas A&M University, College Station, TX, 2017.
- Ekberg A, Kabo E. Fatigue of railway wheels and rails under rolling contact and thermal loading—an overview. *Wear*. 2005;0, no. 7-8 SRC - GoogleScholar:1288-1300.
- Kabo E, Ekberg A. Fatigue initiation in railway wheels—on the influence of defects. *Wear*. 2002;253:26-34.
- Socie DF, Marquis GB. *Multiaxial Fatigue*. Warrendale, PA: Society of Automotive Engineers; 2000.
- Stephens RI, Fatemi A, Stephens RR, Fuchs HO. *Metal Fatigue in Engineering, 2nd ed*. New York, NY: Wiley-Interscience; 2000.
- Bannantine JA, Comer JJ, Handrock JL. Fundamentals of metal fatigue analysis. Englewood Cliffs, NJ: Prentice Hall; 1990:273.
- Fatemi A, Socie DF. A critical plane approach to multiaxial fatigue damage including out-phase loading. *Fatigue &*

- Fracture of Engineering Materials & Structures (FFEMS)*. 1988;11(3):149-165.
31. Park J, Nelson D. Evaluation of an energy-based approach and a critical plane approach for predicting constant amplitude multiaxial fatigue life. *Int J Fatigue*. 2000;22(1):23-39.
32. Jiang Y, Hertel O, Vormwald M. An experimental evaluation of three critical plane multiaxial fatigue criteria. *Int J Fatigue*. 2007;29:1490-1502.
33. Ekberg A, Sotkovszki P. Anisotropy and rolling contact fatigue of railway wheels. *Int J Fatigue*. 2001;23:29-43.

How to cite this article: Kiani M, Fry GT. Fatigue analysis of railway wheel using a multiaxial strain-based critical-plane index. *Fatigue Fract Eng Mater Struct*. 2017;1-13. <https://doi.org/10.1111/ffe.12697>